THE JOURNAL OF PHYSICAL CHEMISTRY B

Article

pubs.acs.org/JPCB

The Minimum Amount of "Matrix" Needed for Matrix-Assisted Pulsed Laser Deposition of Biomolecules

Marshall Tabetah,[†] Andreea Matei,[‡,§] Catalin Constantinescu,[‡,§] Ninell P. Mortensen,[‡,∥] Maria Dinescu,[§] Jørgen Schou,[‡] and Leonid V. Zhigilei*[,†]

[†]Department of Materials Science and Engineering, University of Virginia, 395 McCormick Road, Charlottesville, Virginia 22904-4745, United States

[‡]DTU Fotonik, Technical University of Denmark, DK-4000 Roskilde, Denmark

[§]INFLPR − National Institute for Laser, Plasma and Radiation Physics, 409 Atomistilor Boulevard, Magurele, Bucharest RO-077125, Romania

[∥]RTI International, 3040 Cornwallis Road, Research Triangle Park, North Carolina 27709, United States

Supporting Information

ABSTRACT: The ability of matrix-assisted pulsed laser evaporation (MAPLE) technique to transfer and deposit high-quality thin organic, bioorganic, and composite films with minimum chemical modification of the target material has been utilized in numerous applications. One of the outstanding problems in MAPLE film deposition, however, is the presence of residual solvent (matrix) codeposited with the polymer material and adversely affecting the quality of the deposited films. In this work, we investigate the possibility of alleviating this problem by reducing the amount of matrix in the target. A series of coarse-grained molecular dynamics simulations are performed for a model lysozyme−water system, where the water serves the role of volatile "matrix" that drives the ejection of the biomolecules. The simulations reveal a remarkable ability of a small (5−10 wt %) amount of matrix to cause the ejection of intact bioorganic molecules. The results obtained for different laser fluences and water concentrations are used to establish a "processing map" of the regimes of molecular ejection in matrix-assisted pulsed laser deposition. The computational predictions are supported by the experimental observation of the ejection of intact lysozyme molecules from pressed lysozyme targets containing small amounts of residual water. The results of this study suggest a new approach for deposition of thin films of bioorganic molecules with minimum chemical modification of the molecular structure and minimum involvement of solvent into the deposition process.

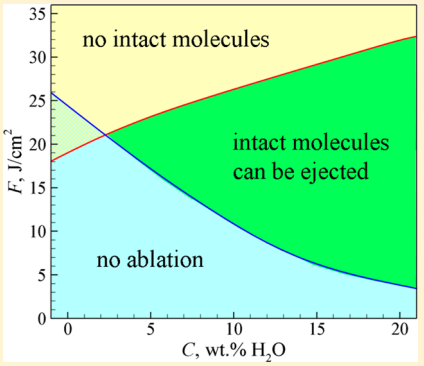

1. INTRODUCTION

The emergence of novel materials and devices that incorporate biomolecule-based components is creating an increasing demand for advanced fabrication methods capable of producing compliant and biologically active organic layers deposited on or embedded in inorganic structures.[1,2] While some specific organic layers for optoelectronic or memory devices have been successfully sandwiched between inorganic layers,[3−5] the fabrication of high-quality thin films and multilayers of intact biomolecules remains challenging. The conventional solution-based techniques, such as spin coating and drop casting, suffer from the lack of thickness control and film nonuniformity due to the uneven wetting of the substrate and solvent evaporation. Pulsed laser deposition (PLD) has been successfully used in fabrication of both inorganic and organic/polymeric thin films,[6,7] but the application of this technique to biomolecules is essentially precluded by unavoidable pyrolytic and/or photolytic fragmentation of molecules in the ablation process.[8−10]

The need for a gentle deposition of ultrathin films of biomolecules retaining their original structure and functionality has led to the development of a technique dubbed matrix-assisted pulsed laser evaporation (MAPLE).[11−13] In MAPLE, the molecules to be deposited are dissolved in a volatile solvent (matrix) and the homogeneous dilute (∼0.1−5 wt %) solution is frozen to produce a target used in the laser deposition setup. Short pulse laser irradiation of the target overheats the matrix to the limit of its thermodynamic stability and results in a collective ejection (ablation) of a surface region of the target driven by an explosive release of matrix vapor in a process described as phase explosion or explosive boiling.[14−16] The volatile matrix is pumped away from the deposition chamber, while the less volatile solute molecules entrained in the expanding plume of matrix molecules are collected on a substrate. Because the conditions for the onset of the phase explosion are defined by the thermodynamic properties of the volatile matrix, the ablation proceeds at temperatures that are sufficiently low to prevent thermal decomposition of the

Received: August 15, 2014
Revised: September 26, 2014
Published: October 27, 2014

   dx.doi.org/10.1021/jp508284n | J. Phys. Chem. B 2014, 118, 13290−13299

deposited molecules. Moreover, the MAPLE technique enables us to have precise control over the average thickness of the deposited film.[17,18] The ability of MAPLE to deposit thin films of polymer and biological molecules without modification of the chemical structure and functionality has led to a rapid expansion of applications of this technique, now ranging from fabrication of optoelectronic and chemical sensing devices to tissue engineering, drug delivery, and medical implantation.[13] The unique capabilities of MAPLE have recently been highlighted by deposition of ultrastable polymer glasses, which cannot be produced by any other method.[19]

The very solvent that provides the conditions for "soft" ejection and deposition of fragile macromolecules in MAPLE, however, can also have a deleterious effect on the quality of the deposited films and presents a number of problems for applications sensitive to solvent contamination.[20] In particular, the rough morphology observed in the majority of MAPLE-deposited films, for example, refs 19−25, bears evidence of an active involvement of solvent in the film growth process and attest against the assumption of complete evacuation of the solvent vapor during its expansion from the irradiated target to the substrate. The characteristic wrinkled surface morphology has been attributed to the interaction of the energetic matrix vapor with the growing film[20] or to the deposition of matrix-solute droplets generated in the ablation process followed by the escape of the trapped matrix vapor.[16,21,26] In the deposition of multilayer structures,[27,28] the transient exposure of already deposited layers to solvent coming with the deposition of subsequent layer(s) may result in undesired dissolution and mixing among the layers. Finally, the MAPLE technique is certainly not compatible with ultrahigh vacuum (UHV) conditions required for fabrication of advanced organic/inorganic heterostructures. Laser irradiation of a frozen target leads to the rapid vaporization of the volatile matrix and causes a pressure increase by more than 2 orders of magnitude. The integration of MAPLE into UHV procedures for fabrication of high-quality organic/inorganic hybrid structures and devices, therefore, is creating demand for elimination or, at least, minimization of the solvent-related effects in MAPLE.

In this Article, we report the results of a computational exploration of the deposition conditions that minimize the required amount of solvent but still produce films composed of intact biomolecules. The minimum amount of matrix needed for the ejection of intact polymer molecules is established in a series of coarse-grained molecular dynamics (MD) simulations performed for different laser fluences. The computational predictions are supported by the experimental observation of the deposition of intact lysozyme molecules from lysozyme targets containing a small amount of residual water. The results of this study suggest a new "inverse MAPLE" approach, where the "matrix/solvent" is a minor component that drives the transfer of intact biomolecules to a substrate.

2. COARSE-GRAINED MD MODEL FOR SIMULATION OF LASER ABLATION OF LYSOZYME−WATER SYSTEM

The conditions leading to the material ejection from polymer targets containing small amounts (from 0 to 20 wt %) of volatile solvent are investigated with a coarse-grained MD model that combines the breathing sphere model developed for simulation of laser interactions with molecular systems[15,29] with the bead-and-spring model commonly used in modeling of polymers and polymer solutions.[16,30] The breathing sphere model adapts a coarse-grained representation of molecules or polymer units by spherical particles that have only one dynamic internal degree of freedom each. The internal degree of freedom is implemented by allowing the particles to change their sizes or to "breathe". The remaining internal degrees of freedom are accounted for through the heat bath approach, in which the breathing motion of each particle is connected to (allowed to exchange energy with) a "heat bath" variable representing all but one of the internal degrees of freedom of the corresponding matrix molecule or polymer unit that are active at a given temperature, that is, contribute to the heat capacity of the molecular system. This approach ensures an adequate representation of the experimental values of heat capacity of the molecular system and allows for the energy exchange between the internal (implicit) and dynamic (explicit) degrees of freedom of the coarse-grained model. At the same time, the coarse-grained representation of both solvent and polymer molecules enables simulations of systems that are sufficiently large to reproduce the collective processes leading to the laser-induced molecular ejection.

To make the computational predictions compatible with the experimental component of this study, the model is parametrized for lysozyme−water system, where the water serves the role of volatile "matrix" that drives the ejection of the lysozyme molecules. The parameters of the model, the heat bath approach that ensures an adequate representation of the experimental values of heat capacity of the molecular systems, and the implementation of the laser energy deposition in the coarse-grained model are described below.

2.1. Parameters of the Inter- and Intramolecular Interactions in the Coarse-Grained Model. In the coarse-grained model, the dynamic unit is a spherical particle that is void of any intramolecular structure, has a mass of M, and is assigned an equilibrium radius, R_0, about which it can expand or contract resulting in a variable radius, $R(t)$. Each coarse-grained particle is, therefore, a breathing sphere that exercises breathing motion about its equilibrium radius in addition to its translational motion. For water, a breathing sphere represents a group of water molecules. For lysozyme, a breathing sphere is a monomer in a polymer chain, that is, a bead in the bead-and-spring model representation.

All intermolecular interactions in the model are described by the Morse potential:[31]

$$U_r(r_{ij}) = D_e\{\exp[-2\beta(r_{ij} - r_e)] - 2\exp[-\beta(r_{ij} - r_e)]\} \quad (1)$$

where $r_{ij} = |\vec{r}_i - \vec{r}_j| - R_i - R_j$ is the distance between edges of particles i and j, $\vec{r}_i$ and $\vec{r}_j$ are positions of the centers of the particles, and R_i and R_j are their instantaneous radii. The parameters of the Morse potential, D_e, β, and r_e, along with the mass M and the equilibrium radius R_0 of a breathing sphere particle, are defining the physical properties of the model material. Note that because the intermolecular potential is defined as a function of the distance between edges of the breathing sphere particles, the effective "size" of the particles (or the equilibrium interparticle distance) is equal to $2R_0 + r_e$.

The breathing motion is controlled by an inertia parameter (or effective mass) M_I ascribed to the corresponding breathing degree of freedom and an anharmonic potential:[29]

$$U_R(R_i) = k_1(R_i - R_0)^2 + k_2(R_i - R_0)^3 + k_3(R_i - R_0)^4 \quad (2)$$

dx.doi.org/10.1021/jp508284n | J. Phys. Chem. B 2014, 118, 13290−13299

where R_i is the instantaneous radius of particle i and k_1, k_2, and k_3 are parameters of the potential. The parameters of this potential control the strength of coupling between the vibrational modes associated with translational motion of the particles and their breathing mode. The choice of the parameters, therefore, can be used to ensure that the rate of the energy equilibration between the optically excited molecules and their surroundings matches the results of pump−probe experiments or atomistic simulations.[15,29]

In the present work, the parameters of the intermolecular potential, eq 1, for the water component are chosen to approximately reproduce room temperature values of density and speed of sound (or bulk modulus), as well as melting temperature and the critical temperature of water. The melting temperature of the model material, T_m, is determined in a constant-pressure and constant-energy liquid−crystal coexistence simulation[32,33] performed for a 81 Å × 81 Å × 242 Å system consisting of 20 736 breathing sphere particles. The system is found to reach the phase equilibrium within 2 ns, and the established temperature provides an estimate of the equilibrium melting temperature of the model material.

The critical temperature of the model material is not rigorously calculated but estimated from the threshold temperature for the onset of explosive boiling (explosive phase separation into liquid and vapor), T^*, determined in a constant zero pressure simulation of slow (0.025 K/ps) heating of a metastable liquid, following an approach applied earlier to other material systems.[16,34,35] The threshold for the explosive boiling is identified from a sharp increase in the volume of the system. The threshold temperature can be expected to be ∼10−20% below the critical temperature.[14,36] Thus, we estimate the critical temperature T_c from the approximate relation $T^* \approx 0.85T_c$.

The following set of parameters, M = 50 Da, R_0 = 0.8 Å, D_e = 0.045 eV, r_e = 3.0 Å, and β = 1.3 Å^{-1}, is found to provide a satisfactory semiquantitative description of experimental properties of water. Some of the properties of the coarse-grained model of water relevant to the ablation phenomenon are listed, along with the experimental values, in Table 1. The water−polymer cross-interactions are described with the same set of parameters of intermolecular potential used for water−water interactions.

Table 1. Properties of the Coarse-Grained Breathing Sphere Model of Water, and the Corresponding Experimental Values[a]

properties of water	experiment	model	error, %
density, ρ, g/cm^3	1.0	1.0	0
bulk modulus, K, GPa	2.2	1.8	18
speed of sound, $c_s = (K/\rho)^{1/2}$, m/s	1483	1342	9
critical temperature, T_c, K	647	588	9
melting temperature, T_m, K	273	330	21

[a]The experimental values are from ref 40.

The parameters of the Morse potential for nonbonding interactions between polymer units are chosen to roughly reproduce the typical strength of nonbonding interactions in proteins and the equilibrium dimensions of a lysozyme globule.[37] For a polymer unit with a mass of M = 111 Da and an equilibrium radius of R_0 = 1.4 Å, the parameters used in the simulations are D_e = 0.15 eV, β = 0.9 Å^{-1}, and r_e = 2.8 Å. With these parameters, a system composed of lysozyme globules arranged into a close-packed structure has a density of 1.83 g/cm^3, whereas a system containing 20 wt % of water has a density of 1.55 g/cm^3. These values are comparable to the experimental density of ∼1.3 g/cm^3 measured for a lysozyme crystal grown in 88% relative humidity and containing ∼17 wt % of water.[38]

The intramolecular "springs" in the bead-and-spring model, corresponding to the chemical bonds between the polymer units, are described by the same Morse potential given by eq 1, with parameters D_e = 3.48 eV, β = 2.37 Å^{-1}, and r_e = 1.54 Å chosen to represent a typical carbon−carbon bond in a polymer molecule.[16]

The parameters of the internal potential given by eq 2 are listed for the water and lysozyme units of the coarse-grained model in Table 2. These parameters ensure that the equilibration time between the translational and breathing modes is ∼30−40 ps for both water and lysozyme at room temperature. The rate of the vibrational equilibration is faster at higher temperatures and under conditions of optical excitation of the breathing mode. Under any conditions, the equilibration time is much shorter than the laser pulse duration of 400 ps used in the simulations.

Table 2. Parameters of the Internal Potential for Water and Lysozyme Components of the Coarse-Grained Model

	M_I, Da	k_1, eV/Å^2	k_2, eV/Å^3	k_3, eV/Å^4
lysozyme	3552	60	−120	120
water	1600	30	−60	60

2.2. Coupling of the Translational Degrees of Freedom to the Breathing Mode and the Heat Bath. Each unit in the coarse-grained model (a breathing sphere or a polymer unit) represents a group of atoms but has only four dynamic degrees of freedom that correspond to the translational and radial breathing motions. The drastically reduced, as compared to real molecular systems, number of dynamic degrees of freedom would lead to substantial underestimation of the heat capacity. To ensure an adequate representation of the experimental values of heat capacity by the coarse-grained model, we use a computational approach based on the introduction of "heat bath" variables representing the energy content of the vibrational modes that are not explicitly represented in the coarse-grained model.[39]

The heat bath variables are associated with all dynamic units of the model. The capacity of a heat bath associated with a dynamic unit, C^{HB}, is obtained by subtracting the contributions of the dynamic degrees of freedom from the fraction of the experimental specific heat due to the group of atoms represented by the dynamic unit, C^{exp}, that is, $C^{HB} = C^{exp} - C^{TR} - C^{R}$, where $C^{TR} = 3k_B$ is the contribution to the heat capacity from the three translational degrees of freedom of the dynamic unit and $C^{R} = k_B$ is the contribution from the radial breathing motion of the unit (k_B is the Boltzmann constant). The heat capacity of water is 4.2 × 10^3 J/(kg K),[40] which translates to a heat capacity of C^{exp} = 2.18 × 10^{-3} eV/K[41] per breathing sphere unit with a mass of 50 Da. The heat capacity of anhydrous lysozyme at 25 °C has been determined to be 1.2 × 10^3 J/(kg K),[42] which translates to a heat capacity of C^{exp} = 1.38 × 10^{-3} eV/K per polymer unit with a mass of 111 Da.

The energy exchange between the internal heat bath variables and the dynamic degrees of freedom of the coarse-grained model is implemented by coupling the heat bath with the

dx.doi.org/10.1021/jp508284n | J. Phys. Chem. B 2014, 118, 13290−13299

breathing motion of the dynamic units of the model. The coupling is realized by scaling the velocities of the radial breathing motion to ensure thermal equilibration between the heat bath and the breathing vibrations. The rate of the equilibration is proportional to the difference between the local temperature of the breathing motion, T_i^R, and the heat bath temperature, T_i^{HB}, of the dynamic unit i. The local breathing temperature at the position of unit i is calculated from the average kinetic energy of breathing motion of units located within the intermolecular potential cutoff distance from the unit i:

$$T_i^R = \sum_{j=1}^{N_i^{loc}} \frac{M_1 (v_j^R)^2}{N_i^{loc} k_B} \quad (3)$$

where $v_j^R = dR_j/dt$ is the instantaneous velocity of the breathing motion of unit j and N_i^{loc} is the number of molecules within the potential cutoff distance from unit i. The potential cutoff distance $r_{ij}^c = 10$ Å, defined as the distance between edges of the breathing sphere particles, is used in this work.

To ensure the energy conservation, the energies of the heat bath and the breathing motion are changed at each time-step of the integration of the equations of motion of the dynamic units with rates of the same magnitude but opposite sign:

$$C^R \frac{dT_i^R}{dt} = A(T_i^{HB} - T_i^R),\ C_i^{HB} \frac{dT_i^{HB}}{dt} = -A(T_i^{HB} - T_i^R) \quad (4)$$

where A is a constant that controls the rate of the energy exchange. The transfer of energy to/from the breathing vibrational mode is followed by the fast equilibration with the translational degrees of freedom that are dynamically coupled to the breathing motion, as described above in section 2.1.

From eq 4, the constant A can be related to the characteristic time τ of the energy exchange between the heat bath and the breathing mode, defined as a time constant of the exponential decay of the temperature difference between T_i^{HB} and T_i^R, as $A = [(C_i^{HB}C^R)/(C_i^{HB} + C^R)]1/\tau$. Because the energy transferred to the breathing mode is simultaneously redistributed to the translational modes through the dynamic coupling, the total heat capacity of the dynamic degrees of freedom of the model, $C^{TR} + C^R$, should be used instead of C^R in the expression connecting the constant A and the equilibration time τ, that is, $A = [C_i^{HB}(C^{TR} + C^R)/(C_i^{HB} + C^{TR} + C^R)]1/\tau$. Finally, because $C_i^{HB} \gg C^{TR} + C^R$, an approximate relation $A \approx (C^{TR} + C^R)/\tau$ can be used to estimate the value of A that yields a desired value of τ. In this work, we aim at $\tau \approx 20$ ps and use $A = 1.7 \times 10^{-5}$ eV K^{-1} ps^{-1}. As a result, the vibrational relaxation of the excited molecules, proceeding in the model through the energy transfer from the heat bath to the breathing motion and through the dynamic coupling between the breathing and translational modes, takes time on the order of several tens of picoseconds, consistent with the time scale of vibrational energy relaxation in proteins determined in atomistic simulations and measured in pump–probe experiments.[43−45]

2.3. Simulation of the Laser Excitation. The laser wavelength of 355 nm, pulse duration of 400 ps, and laser fluence ranging from 3 to 35 J/cm^2 are used in the simulations. Here and below, the absorbed/transmitted laser fluence F, related to the incident fluence as $F = F_{inc}(1 - R)$, where R is the reflectivity of the target surface, is used in the presentation of the simulation results. The laser excitation at a wavelength of 355 nm is simulated by deposition of quanta of energy equal to the photon energy (3.5 eV) into the heat bath energy of the dynamic units of the model that are randomly chosen during the laser pulse duration. The total number of photons entering the model during the laser pulse is determined by the laser fluence, and the probability of a molecule to be excited is modulated by Lambert−Beer's law to reproduce the exponential attenuation of the laser light with depth. The laser penetration depth of ∼30 μm is used in the simulations. This value is determined in experiments performed for a dry 100 μm thick lysozyme layer confined between two quartz windows and irradiated with a low-energy laser pulse. The depth of a visible darkening is used as an estimate of the laser penetration depth. The absorption by water is negligible (penetration depth of pure water is ∼25 m at 355 nm, ref 46), and the effective values of the laser penetration depth for targets with water pockets are 33 μm for 5 wt % water, 36 μm for 10 wt % water, 40 μm for 15 wt % water, and 45 μm for 30 wt % water.

The laser penetration depth of 30−45 μm is much larger than the thickness of the simulated target, ∼45 nm. The laser energy deposition, therefore, results in even heating throughout the thickness of the target. The pulse duration of 400 ps is shorter than the experimental value of 6 ns, but is still sufficiently long to ensure that the same physical regime of thermal but not stress confinement[15,16] is realized in both the simulations and the experiments. The photothermal bond breaking in the model is homolytic (thermally activated scission of 3.48 eV bonds in the polymer chains). Heterolytic bond breaking (1−2 eV) is not included in the model, which may result in overestimation of the values of fluence needed for the molecular decomposition.

2.4. Parameters of Simulated Targets. The system used in the simulations is a 44.8 nm thick lysozyme target containing small pockets of residual water and deposited on a transparent substrate. In the case of pure lysozyme system, Figure 1a, the target consists of 1296 lysozyme chains arranged in globular conformations, with material density of 1.83 g/cm^3. Each globule has 129 monomer units representing amino acid residues of the chicken egg-white lysozyme,[47] with a mass of a unit being 111 Da (14 307 Da/129 ≈ 111 Da). The individual globules are produced by allowing polymer chains with initial random conformations to relax in a MD simulation performed with free boundary conditions. The globules are then arranged in a close-packed crystal and equilibrated in a simulation performed at zero pressure and 300 K. Following the equilibration, the substrate and a free surface are introduced, the dimensions of the computational cell in the directions parallel to the surface are fixed at 11.2 × 33.6 nm^2, and the periodic boundary conditions are applied in these directions. The interaction between the polymer molecules and the rigid optically transparent substrate at the bottom of the computational cell is assumed to be 3 times stronger than the nonbonded intermolecular interactions. In the simulations of systems with residual water, small (∼3 nm) water pockets are randomly distributed in the target. The density of the targets with water is 1.75, 1.68, 1.62, and 1.55 g/cm^3 for systems with water concentrations of 5, 10, 15, and 20 wt %, respectively.

3. RESULTS OF MD SIMULATIONS

The results of two representative simulations performed for pure lysozyme targets are illustrated in Figure 1b−d. The time dependences of the fractions of broken bonds and the remaining intact molecules shown in Figure 1b indicate that

dx.doi.org/10.1021/jp508284n | J. Phys. Chem. B 2014, 118, 13290−13299

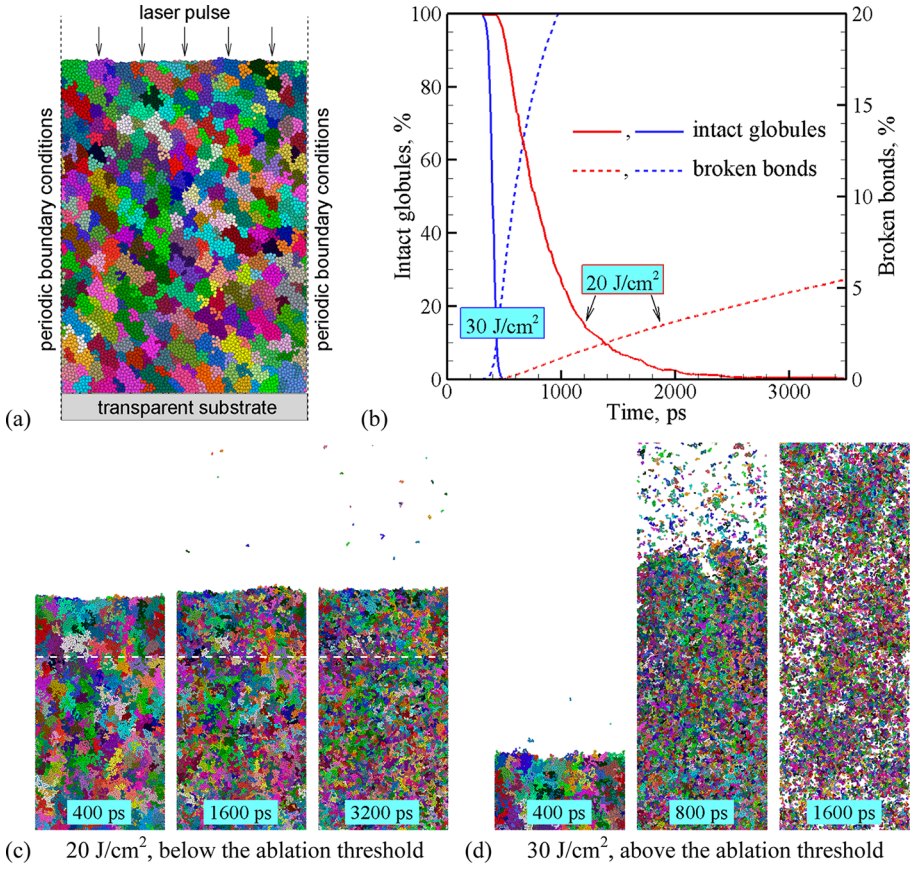

Figure 1. Schematic sketch of the simulation setup for modeling of laser irradiation of pure lysozyme targets on a transparent substrate (a) and the results of two simulations performed at laser fluences of 20 and 30 J/cm^2, that is below and above the ablation threshold, respectively (b–d). The laser pulse duration is 400 ps. The evolution of the fraction of broken chemical bonds and the number of intact polymer molecules is shown in (b). Snapshots of molecular configurations are shown in (c,d). Individual globular molecules in (a) are colored by different random color. The same color is used for molecular fragments originating from the same molecule in (c,d). The regions shown in the snapshots in (c,d) have heights of 100 nm and are located just above the substrate in (c) and 60 nm above the substrate in (d). The white dashed lines in (c) mark the initial position of the surface of the target before the laser irradiation.

even at the lower fluence of 20 J/cm^2 the thermally activated bond scission leads to the complete decomposition of all molecules by the time of 2.5 ns. Snapshots from this simulation (Figure 1c), however, clearly demonstrate that the fluence of 20 J/cm^2 is below the threshold of the collective material ejection (ablation) and the molecular ejection is limited to desorption of several small molecular fragments. The ablation does take place at a higher fluence of 30 J/cm^2, when a rapid release of small volatile fragments generated in the pyrolytic decomposition of polymer molecules drives the ejection of the larger polymer fragments and molecular droplets, Figure 1d. The molecular fragmentation in this case is more rapid and leaves no intact molecules by the time of 0.5 ns. The results of the simulations performed for pure lysozyme targets are consistent with the well-established understanding[8−10] that the dissociation of a large fraction of chemical bonds is a required step of the polymer ablation and no ejection of intact molecules can be expected in PLD.

The presence of small water pockets randomly distributed in the lysozyme targets makes a surprisingly strong impact on the processes induced by the laser irradiation, even when the average concentration of water is rather minute. In particular, an addition of only 10 wt % of water leads to the drop in the fluence threshold for the ablation onset by more than a factor of 2, from ∼24 J/cm^2 for the pure lysozyme target to ∼11 J/cm^2. The snapshots for simulations performed at fluences just below and above the ablation threshold, Figure 2b and c, clearly demonstrate the prominent role the water content plays in driving the ablation process. At 8 J/cm^2, the rapid vaporization of water pockets results in the film expansion and generation of large bubbles filled with superheated water vapor during the first 2 ns after the start of the laser pulse, Figure 2b. The driving force provided by the expanding bubbles, however, is not sufficient for the ejection of entangled lysozyme molecules. At 2.3 ns, a large bubble in the surface region bursts, releases the water molecules, and gradually deflates. The surface of the target recesses, and no lysozyme ejection is observed in this simulation. At a higher fluence of 13 J/cm^2, however, the expanding water vapor breaks the resistance of the interconnected viscous network of lysozyme molecules, entrains droplets of polymer material, and results in the ejection of almost the entire target.

Even more striking than the sharp drop in the ablation threshold is the observation that not a single chemical bond is broken and all lysozyme molecules are ejected intact in the simulations performed for films with 10 wt % water at fluences close to the ablation threshold, 10 and 13 J/cm^2. At 16 J/cm^2, the molecular fragmentation is still negligible, and only 0.2% of molecules are fragmented by the end of the simulation. A noticeable fragmentation is observed only at 21 J/cm^2 (twice

dx.doi.org/10.1021/jp508284n | J. Phys. Chem. B 2014, 118, 13290−13299

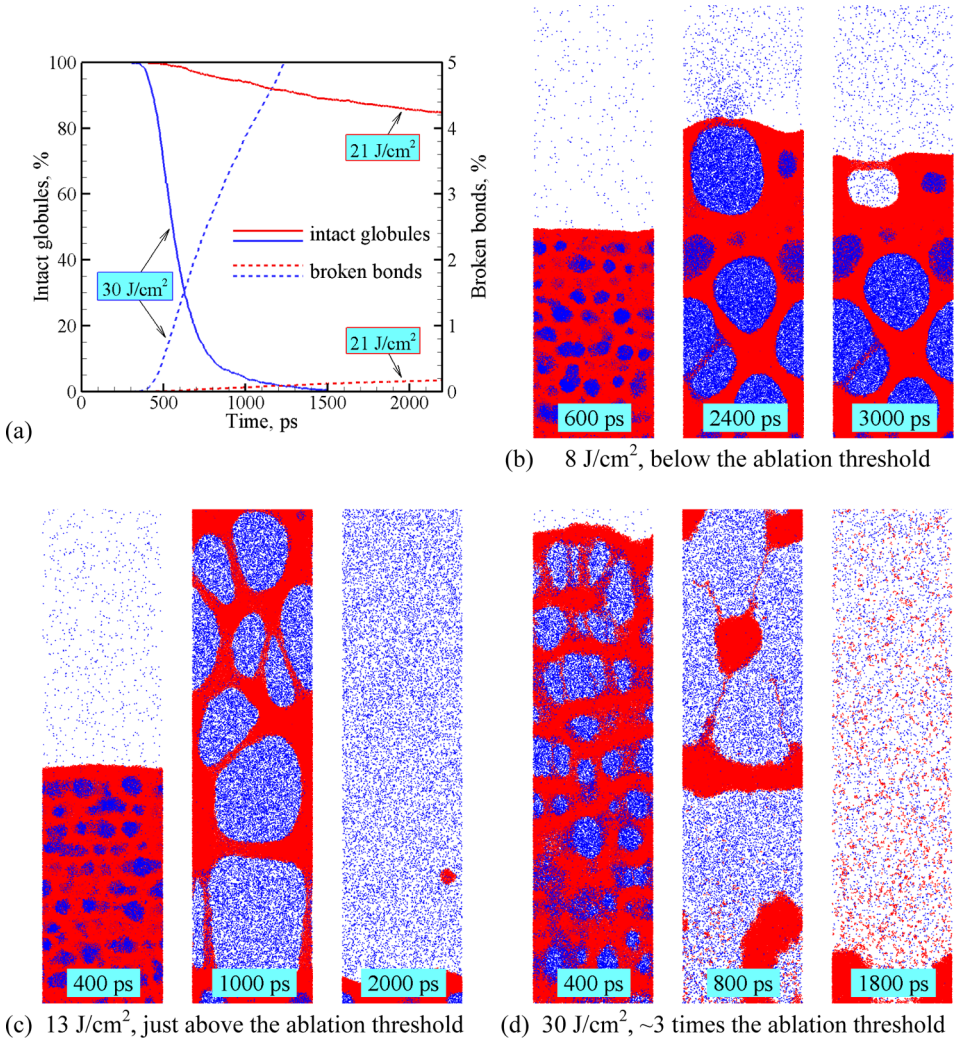

Figure 2. Results of simulations of 400 ps laser pulse irradiation of a thin lysozyme target containing 10 wt % of residual water. The evolution of the fraction of broken chemical bonds and the number of intact lysozyme molecules is shown in (a) for fluences of 21 and 30 J/cm^2. No bond scission is observed in simulations performed at fluences below 16 J/cm^2. Snapshots of molecular configurations obtained in simulations performed at laser fluences of 8, 13, and 30 J/cm^2 are shown in (b), (c), and (d), respectively. The units of polymer chains and water molecules are shown as red and blue particles, respectively.

the ablation threshold), Figure 2a, where the slowly increasing fraction of broken bonds reaches 0.23% and the fraction of fragmented lysozyme molecules reaches 20% by the time of 3 ns. We recall that a molecule is fragmented if just one bond out of the 128 bonds in the molecule is cut. The time dependences of the fractions of broken bonds and intact molecules show signs of saturation by 3 ns, and one can expect that more than 50% of lysozyme molecules will survive the ejection process at this fluence. At a higher fluence of 30 J/cm^2 (almost 3 times the ablation threshold), the fragmentation is extensive, the fraction of the broken bonds reaches 6%, and all lysozyme molecules are fragmented by the time of 2 ns; see Figure 2a. The ejection of large polymer droplets in this case is driven by the expansion of a mixture of water vapor and small volatile products of polymer thermal decomposition (blue dots and red fragments in the snapshot shown for 1800 ps in Figure 2d, respectively).

Simulations similar to the ones discussed above for targets with 10 wt % water have also been performed for smaller (5 wt %) and higher (15, 20, and 30 wt %) water content. The results of the simulations are summarized in the fluence–water concentration map of the molecular ejection regimes shown in Figure 3. The decrease of the ablation threshold with increasing water concentration, shown by the blue line in the figure, is reflecting the prominent role the water vapor plays in driving the collective ejection of the polymer droplets. In the absence of water (C = 0 wt % H_2O), the ablation is driven by the rapid release of the volatile products of thermal decomposition of lysozyme molecules, which occurs at temperatures exceeding ~3700 K (see Supporting Information) and inevitably destroys all of the molecules. In the presence of water pockets, the rapid vaporization of water is driving the material ejection, and the maximum temperature of the target at the ablation threshold decreases with increasing water content to about 2500, 1750, 1000, 750, and 650 K at water concentrations of 5, 10, 15, 20, and 30 wt % H_2O, respectively.

The vaporization of water pockets and the rapid expansion of the target material are also providing alternative conduits for channeling some of the energy deposited by the laser pulse away from the pyrolytic decomposition of lysozyme molecules, thus leading to the gradual increase of the threshold fluence for complete molecular decomposition shown by the red curve in Figure 3. As a result, while no possibility for the ejection of

dx.doi.org/10.1021/jp508284n | J. Phys. Chem. B 2014, 118, 13290–13299

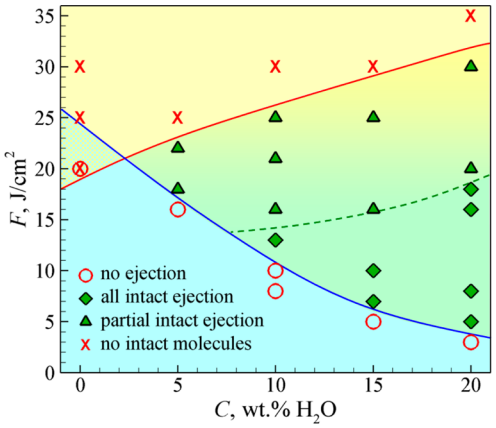

Figure 3. Laser fluence–water concentration map of distinct regimes of molecular ejection observed in simulations of 400 ps laser pulse irradiation of lysozyme targets containing different amounts of residual water. The blue line shows the ablation threshold; the data points below this line are for simulations where the molecular ejection is limited to desorption of water molecules and/or small volatile molecular fragments. The red line shows the threshold for complete decomposition of the lysozyme molecules; no intact molecules survive the laser irradiation in simulations that correspond to the data points above this line. The green "◆", "▲" are for simulations where the ejection of intact lysozyme molecules is observed, with the green dashed line separating the domains of partial and complete survival of the molecules.

intact molecules exists to the left of the intersection of the blue and red curves (essentially, in the PLD regime), an expanding "window of opportunities" for the ejection of intact molecules appears to the right of the intersection and is outlined by the two curves. Moreover, the simulations predict the possibility of low-fluence ablation of thin molecular films with complete absence of thermally activated bond scission (the region between the solid blue and dashed green lines).

4. EXPERIMENTAL RESULTS ON DEPOSITION OF INTACT LYSOZYME MOLECULES

The computational predictions can be related to the results of laser deposition experiments performed for a target of pressed chicken egg white lysozyme powder. The target was irradiated by a Nd:YAG laser at a repetition rate of 1 Hz, laser wavelength of 355 nm, and pulse width of 6 ns with an angle of incidence of 45° and in a distance of 60 mm from the substrate, typically the electrode of an oscillating quartz crystal microbalance. The film deposition rate per pulse in a vacuum was measured with the quartz crystal microbalance with a sensitivity of 1 Hz corresponding to 1.3×10^{16} amu/cm^2. Each deposition was done with a rastering beam to avoid hole-drilling in the pressed (dry) lysozyme target. The deposition rate is plotted as a function of fluence in Figure 4a. The rate increases slowly up to 1.2 J/cm^2 and more sharply for higher fluences. The rate is 5.3 ng/cm^2 per pulse at a typical PLD fluence of 2 J/cm^2. For the repetition rate of 1 Hz and the lysozyme crystal density of 1.24 g/cm^3,[48] this deposition rate corresponds to a lysozyme film with an average thickness of 77 nm produced in a half an hour deposition.

The bioactivity of lysozyme molecules in two films produced with 21 600 pulses at 2 J/cm^2 was confirmed by tests with the EnzChek Lysozyme Assay Kit (E22 013) supplied by "Invitrogen". With this assay, the lysozyme activity on *Micrococcus lysodeikticus* cell walls induces a fluorescence, which was detected for both films, similar to what we found for films produced by MAPLE.[17]

While feasible films can be conveniently produced by PLD, the next issue is whether the films contain a significant amount of intact molecules. This question is addressed by quantitative matrix-assisted laser desorption ionization (MALDI) analysis of the deposited films. For MALDI studies, thin films of the protein were deposited on 7 × 7 mm^2 Si-⟨100⟩-wafers. The thickness of the films was the same, ~140 nm (17.2×10^3 ng/cm^2), at all laser fluences. To prepare a MALDI sample, a film was placed on a stainless steel plate, a drop of 0.5 μL of the MALDI matrix was poured onto the film, and the resulting solution was dried in a vacuum (10^{-6} mbar). The MALDI matrix was a solution of 70 mg of sinapinic acid, 2 mL of acetonitrile, and 1 mL of water with 0.1% trifluoroacetic acid (TFA). For the nonirradiated material (i.e., lysozyme powder), the lysozyme was dissolved in ultrapure water, and the solution was mixed with the MALDI matrix so that the same ratio between lysozyme and matrix (10^{-4}) is maintained.

The MALDI spectra obtained for the samples produced from the original lysozyme target material and from the films deposited at different laser fluences are shown in Figure 5. The spectra demonstrate that, within the investigated range of fluences, a considerable fraction of the lysozyme molecules are transferred in the laser deposition without fragmentation. The spectra from all MALDI samples look similar to a standard lysozyme MALDI spectrum, with the peaks for singly charged protonated lysozyme $[M + H]^+$ at (14 307 + 1) Da, double mass ions $[2M + H]^+$ at (28 614 + 1) Da, and doubly charged molecular ion $[M + 2H]^{2+}$ at M/z = (7153.5 + 1) Da/charge present in all spectra, where M is the molecular mass and z is the charge. The quantitative analysis of the spectra has been carried out by integrating, after background subtraction, the MALDI signal for a mass of 14 307 Da. The analysis has been carried out with the same setting of the nitrogen laser of the MALDI system, the same parameters of the mass detection system, and the same number of the laser shots. Because all MALDI samples to be analyzed were prepared with the same matrix and had the same thickness, the only parameter that was varied was the laser ablation fluence used in the deposition of the films. The integrated signal, therefore, reflects the relative amount of intact molecules after background subtraction.

The results of the MALDI analysis of films deposited at different laser fluences are shown in Figure 4b. The fraction of the intact molecules in the deposited films is increasing with fluence, reaches the maximum at ~2.5 J/cm^2, and drops at higher fluences. The transfer of a considerable amount of intact lysozyme molecules to the substrate in a matrix-free deposition is unexpected for the PLD conditions and appears to contradict the computational prediction discussed above. Moreover, the initial increase in the yield of intact molecules with increasing fluence is also surprising as a more extensive molecular fragmentation can be expected at higher energy densities generated in the irradiated target by a stronger laser excitation.

A clue to explaining the experimental observations is provided by the results of thermogravimetric analysis of the lysozyme target shown in Figure 4c. The shapes of the TG and DTG curves indicate that prior to the thermal decomposition of lysozyme molecules at T > 200 °C, there is about 8 wt % mass loss in the temperature range of ~40–130 °C that can be attributed to the release of the residual water. The presence of water in the "dry" lysozyme targets is not surprising as the solvent content of native lysozyme crystals exceeds 30% by

dx.doi.org/10.1021/jp508284n | J. Phys. Chem. B 2014, 118, 13290–13299

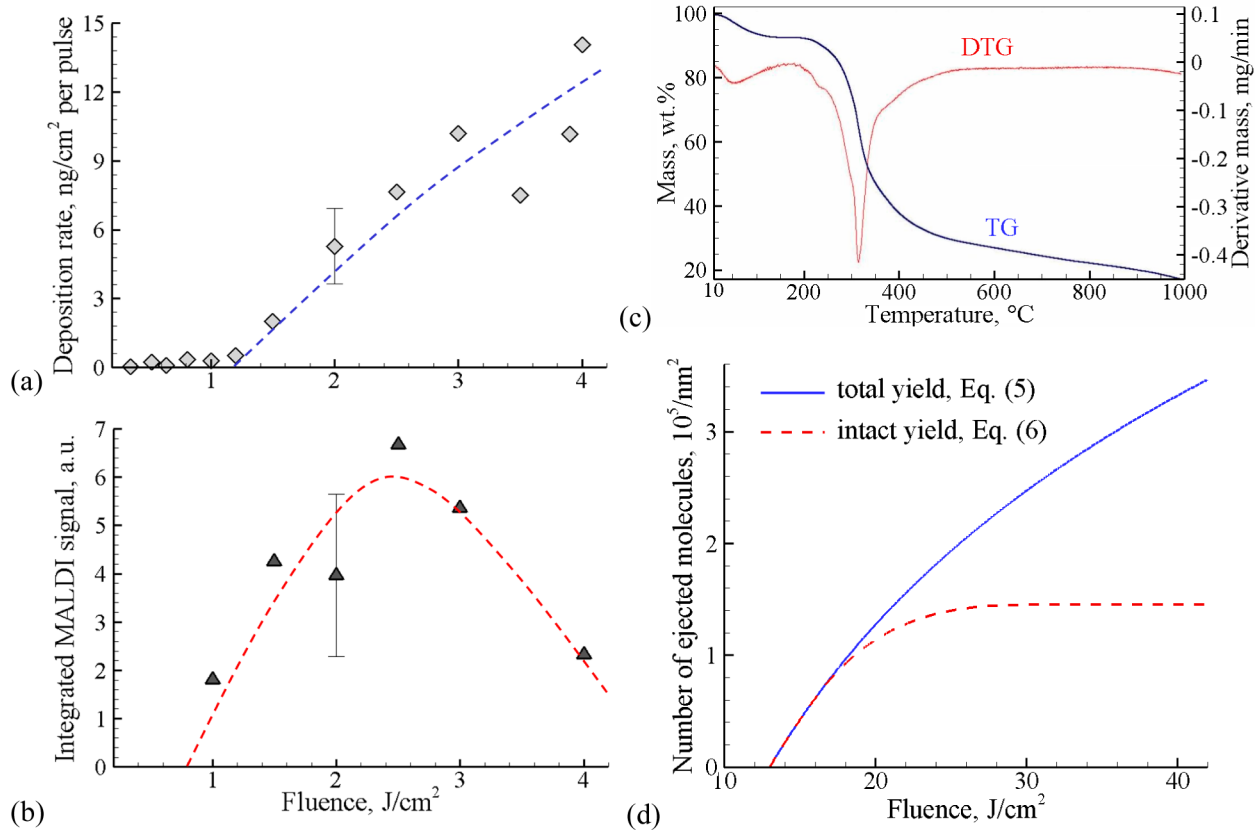

Figure 4. (a,b) The deposition rate per pulse as a function of laser fluence in experiments performed for a lysozyme target irradiated in vacuum with 6 ns pulses at 355 nm (a), the relative integrated MALDI signal for mass 14 307 Da obtained for the deposited films with the same thickness corresponding to 17.2×10^3 ng/cm^3 (b). The dashed lines in (a,b) are given as guides to the eye. (c) The results of thermogravimetric analysis of a lysozyme target used in the laser deposition experiments. The thermogravity (TG) and derivative thermogravity (DTG) curves show about 8% mass loss at $T < 150$ °C attributable to the residual water, followed by decomposition of lysozyme at higher temperature. (d) The laser fluence dependences of the total yield in ablation of a bulk lysozyme target and the yield of intact molecules predicted by eqs 5, 6 with parametrization based on the results of MD simulations performed for a lysozyme target containing 10 wt % of residual water. The yield is given as the number of lysozyme molecules ejected per nm^2 (water excluded); the lysozyme number density in the target with 10 wt % water, $n_m = 8.2$ nm^3, is used in the calculations.

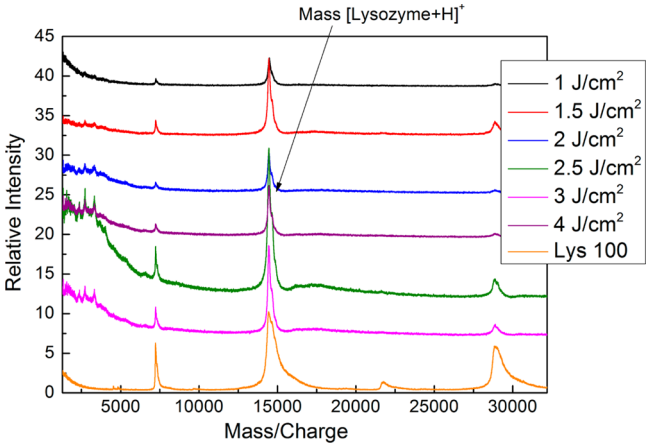

Figure 5. MALDI spectra obtained for the original lysozyme material used as a target in laser deposition (orange curve at the bottom) and for the films deposited at different laser fluences.

volume, remains at 9.4% in crystals prepared in relatively dehydrated conditions (relative humidity of 5%),[38] and can actually be much larger in aqueous solvent.[49] According to the "processing map" predicted in the simulations, Figure 3, the presence of ~8 wt % of residual water may create conditions amenable for the ejection and deposition of intact molecules. The distinction between the thin film of lysozyme molecules deposited on a transparent substrate used in the simulations and the bulk target used in the experiments, however, calls for further analysis provided below.

5. CONNECTIONS BETWEEN EXPERIMENTS AND SIMULATIONS

The connections between the computational predictions for the thin films and the experimental observations for bulk targets can be established by mapping the values of the deposited laser energy density in the simulations performed at different fluences to the energy density distribution with depths in an irradiated bulk target. For the bulk target, we assume a model in which the ablation depth z^* follows the laser energy deposition and the region of the target that absorbs an energy density higher than a critical energy density, ε^*, is ablated.[8,15,16,29] With an exponential decay of the laser intensity given by Beer's law, the energy density deposited by the laser pulse at a depth z is $\varepsilon(z) = (F/L_p) \exp(-z/L_p)$, where L_p is the laser penetration depth and F is the absorbed laser fluence. This energy is added to the thermal energy of the sample equilibrated at 300 K. The ablation yield expressed in terms of the number of molecules ejected from unit surface area then is

dx.doi.org/10.1021/jp508284n | J. Phys. Chem. B 2014, 118, 13290−13299

$$Y^{tot} = n_m z^* = n_m L_p \ln\left(\frac{F}{L_p \varepsilon^*}\right) \quad (5)$$

where n_m is the molecular number density.

Because the thickness of the films used as targets in the simulations is almost 3 orders of magnitude smaller than L_p, the energy density ε^F deposited by the laser pulse with fluence F can be well approximated as the energy density deposited at the surface of the target, that is, $\varepsilon^F = F/L_p$. The results of the MD simulations thus provide us with an estimate of the fraction of the intact molecules that survive the ejection process at a given energy density deposited by the laser, $f(\varepsilon^F)$. For the experimental conditions of laser ablation of a bulk target, the number of ejected intact molecules per unit area, Y^{int}, can be obtained through integration of the fraction of intact molecules ejected from different depths under the irradiated surface:

$$Y^{int} = n_m \int_0^{z^*} f[\varepsilon(z)]\, dz \quad (6)$$

where the limits of integration are from the surface of the sample, $z = 0$, to the ablation depth z^* given by eq 5.

The results of the calculation of Y^{tot} and Y^{init} for a target containing 10 wt % of residual water are shown in Figure 4d. While the total yield increases logarithmically, the yield of intact molecules saturates at a constant value above ~30 J/cm^2, about 3 times the ablation threshold. The predicted fraction of the intact molecules in the ablation plume (Y^{init}/Y^{tot} in Figure 4d), therefore, decreases at high fluencies, which qualitatively agrees with the experimental observations, Figure 4b. Moreover, the observation that the intact molecules constitute the lower part of the ejected plume and have smaller ejection velocities[15,16] suggests that some of the molecules can be pushed back by the more energetic upper part of the plume and redeposited to the target.[50] The redeposition would result in an even sharper decrease of the fraction of intact molecules at higher fluences, as observed in the experiments, Figure 4b.

The substantially higher, as compared to the experimental measurements, values of the ablation threshold fluence in the simulations can be attributed to several factors. The higher density of the simulated targets, 1.55−1.83 g/cm^3, versus 0.73 g/cm^3 of the samples used in experiments, results in a smaller energy deposited per molecule at the same laser fluence and penetration depth. Moreover, the multipulse irradiation of the target in the experiments may lead to damage accumulation and may increase the effective absorption of the surface region of the target. Finally, as discussed above, the thermal decomposition of lysozyme molecules is likely to involve bond breaking mechanisms with activation barriers lower than 3.48 eV assumed in the model. The combination of these factors can well account for the higher values of the laser fluence required for the onset of both the ablation and the active molecular decomposition.

6. CONCLUSION

The computational prediction and the experimental confirmation of the ability of the amounts of solvent as small as 5−10 wt % to cause ejection and deposition of intact polymer molecules suggest a new approach for deposition of thin films of bioorganic molecules with minimum chemical modification of the molecular structure and minimum involvement of solvent into the deposition process. The map of the regimes of molecular ejection obtained in the simulations demonstrates an existence of a range of irradiation conditions suitable for deposition of intact biomolecules at relatively small solvent concentrations. While this map is produced for a particular system (a thin lysozyme target with residual water), the physical picture emerging from this study can be generalized to other systems where a small amount of volatile solvent can provide the driving force for the ejection of heat-sensitive bioorganic material with minimum chemical modification. The deposition in this case is essentially an "inverse MAPLE" process, as the ratio of the deposited material to the "matrix" in the target can be as high as 10:1 instead of the typical 1:100 in the conventional MAPLE deposition. This approach may enable deposition of high-quality bioorganic films suitable for nanomedicine, bioelectronics, and tissue engineering, where minimization of the interaction of solvent with the deposited films is required.

■ ASSOCIATED CONTENT

Supporting Information

Contour plots illustrating the evolution of temperature and density in simulations of pure lysozyme targets (Figure S1) and targets containing 10 wt % of residual water (Figure S2). This material is available free of charge via the Internet at http://pubs.acs.org.

■ AUTHOR INFORMATION

Corresponding Author

*Tel.: (434) 243-3582. Fax: (434) 982-5660. E-mail: lz2n@virginia.edu.

Notes

The authors declare no competing financial interest.

■ ACKNOWLEDGMENTS

We thank Robert Standaert, Chengping Wu, and Jing Zou for helpful discussions and Petre Rotaru for help provided with the thermal analysis of lysozyme samples. Financial support for this work was provided by the National Science Foundation through Grants DMR-0907247 and CMMI-1301298.

■ REFERENCES

(1) Alivisatos, P.; Barbara, P. F.; Castleman, A. W.; Chang, J.; Dixon, D. A.; Klein, M. L.; McLendon, G. L.; Miller, J. S.; Ratner, M. A.; Rossky, P. J.; et al. From Molecules to Materials: Current Trends and Future Directions. *Adv. Mater.* **1998**, *10*, 1297−1336.

(2) Guha, S.; Adil, D.; Ukah, N. B.; Gupta, R. K.; Ghosh, K. MAPLE-Deposited Polymer Films for Improved Organic Device Performance. *Appl. Phys. A: Mater. Sci. Process.* **2011**, *105*, 547−554.

(3) Lindner, F.; Walzer, K.; Leo, K. Organic Heterostructure Device with Nonvolatile Memory Behavior Using Electrically Doped Layers. *Appl. Phys. Lett.* **2008**, *93*, 233305.

(4) Hoven, C. V.; Garcia, A.; Bazan, G. C.; Nguyen, T.-Q. Recent Applications of Conjugated Polyelectrolytes in Optoelectronic Devices. *Adv. Mater.* **2008**, *20*, 3793−3810.

(5) Siebeneicher, P.; Kleemann, H.; Leo, K.; Lüssem, B. Non-volatile Organic Memory Devices Comprising SiO_2 and C_{60} Showing 10^4 Switching Cycles. *Appl. Phys. Lett.* **2012**, *100*, 193301.

(6) Chrisey, D. B., Hubler, G. K., Eds. *Pulsed Laser Deposition of Thin Films*; Wiley-Interscience: New York, 1994.

(7) Eason, R., Ed. *Pulsed Laser Deposition of Thin Films: Applications-Led Growth of Functional Materials*; Wiley-Interscience: Hoboken, NJ, 2007.

(8) Srinivasan, R.; Braren, B. Ultraviolet Laser Ablation of Organic Polymers. *Chem. Rev.* **1989**, *89*, 1303−1316.

(9) Bityurin, N.; Luk'yanchuk, B. S.; Hong, M. H.; Chong, T. C. Models for Laser Ablation of Polymers. *Chem. Rev.* **2003**, *103*, 519−552.
(10) Prasad, M.; Conforti, P. F.; Garrison, B. J. On the Role of Chemical Reactions in Initiating UV Ablation in Poly (methyl methacrylate). *J. Appl. Phys.* **2007**, *101*, 103113.
(11) Piqué, A.; McGill, R. A.; Chrisey, D. B.; Leonhardt, D.; Mslna, T. E.; Spargo, B. J.; Callahan, J. H.; Vachet, R. W.; Chung, R.; Bucaro, M. A. Growth of Organic Thin Films by the Matrix Assisted Pulsed Laser Evaporation (MAPLE) Technique. *Thin Solid Films* **1999**, *355/356*, 536−541.
(12) Chrisey, D. B.; Piqué, A.; McGill, R. A.; Horwitz, J. S.; Ringeisen, B. R.; Bubb, D. M.; Wu, P. K. Laser Deposition of Polymer and Biomaterial Films. *Chem. Rev.* **2003**, *103*, 553−576.
(13) Special Issue on Matrix-Assisted Pulsed Laser Evaporation: Fundamentals and Applications. *Appl. Phys. A: Mater. Sci. Process.* **2011**, *105*, 517−671.
(14) Miotello, A.; Kelly, R. Laser-Induced Phase Explosion: New Physical Problems When a Condensed Phase Approaches the Thermodynamic Critical Temperature. *Appl. Phys. A: Mater. Sci. Process.* **1999**, *69*, S67−S73.
(15) Zhigilei, L. V.; Leveugle, E.; Garrison, B. J.; Yingling, Y. G.; Zeifman, M. I. Computer Simulations of Laser Ablation of Molecular Substrates. *Chem. Rev.* **2003**, *103*, 321−348.
(16) Leveugle, E.; Zhigilei, L. V. Molecular Dynamics Simulation Study of the Ejection and Transport of Polymer Molecules in Matrix-Assisted Pulsed Laser Evaporation. *J. Appl. Phys.* **2007**, *102*, 074914.
(17) Purice, A.; Schou, J.; Kingshott, P.; Dinescu, M. Production of Active Lysozyme Films by Matrix Assisted Pulsed Laser Evaporation at 355 nm. *Chem. Phys. Lett.* **2007**, *435*, 350−353.
(18) Matei, A.; Schou, J.; Constantinescu, C.; Kingshott, P.; Dinescu, M. Growth of Thin Films of Low Molecular Weight Proteins by Matrix Assisted Pulsed Laser Evaporation (MAPLE). *Appl. Phys. A: Mater. Sci. Process.* **2011**, *105*, 629−633.
(19) Guo, Y.; Morozov, A.; Schneider, D.; Chung, J. W.; Zhang, C.; Waldmann, M.; Yao, N.; Fytas, G.; Arnold, C. B.; Priestley, R. D. Ultrastable Nanostructured Polymer Glasses. *Nat. Mater.* **2012**, *11*, 337−343.
(20) Caricato, A. P.; Arima, V.; Cesaria, M.; Martino, M.; Tunno, T.; Rinaldi, R.; Zacheo, A. Solvent-Related Effects in MAPLE Mechanism. *Appl. Phys. B: Laser Opt.* **2013**, *113*, 463−471.
(21) Leveugle, E.; Sellinger, A.; Fitz-Gerald, J. M.; Zhigilei, L. V. Making Molecular Balloons in Laser-Induced Explosive Boiling of Polymer Solutions. *Phys. Rev. Lett.* **2007**, *98*, 216101.
(22) Pate, R.; Stiff-Roberts, A. D. The Impact of Laser-Target Absorption Depth on the Surface and Internal Morphology of Matrix-Assisted Pulsed Laser Evaporated Conjugated Polymer Thin Films. *Chem. Phys. Lett.* **2009**, *477*, 406−410.
(23) Bubb, D. M.; Corgan, J.; Yi, S. Y.; Khan, M.; Hughes, L.; Gurudas, U.; Papantonakis, M.; McGill, R. A. An Experimental Investigation of Inhomogeneities in Resonant Infrared Matrix-Assisted Pulsed-Laser Deposited Thin Polymer Films. *Appl. Phys. A: Mater. Sci. Process.* **2010**, *100*, 523−531.
(24) Caricato, A. P.; Leggieri, G.; Martino, M.; Vantaggiato, A.; Valerini, D.; Cretì, A.; Lomascolo, M.; Manera, M. G.; Rella, R.; Anni, M. Dependence of the Surface Roughness of MAPLE-Deposited Films on the Solvent Parameters. *Appl. Phys. A: Mater. Sci. Process.* **2010**, *101*, 759−764.
(25) Shepard, K. B.; Guo, Y.; Arnold, C. B.; Priestley, R. D. Nanostructured Morphology of Polymer Films Prepared by Matrix Assisted Pulsed Laser Evaporation. *Appl. Phys. A: Mater. Sci. Process.* **2013**, *110*, 771−777.
(26) Zhigilei, L. V.; Volkov, A. N.; Leveugle, E.; Tabetah, M. The Effect of the Target Structure and Composition on the Ejection and Transport of Polymer Molecules and Carbon Nanotubes in Matrix-Assisted Pulsed Laser Evaporation. *Appl. Phys. A: Mater. Sci. Process.* **2011**, *105*, 529−546.
(27) Califano, V.; Bloisi, F.; Vicari, L. R. M.; Colombi, P.; Bontempi, E.; Depero, L. E. MAPLE Deposition of Biomaterial Multilayers. *Appl. Surf. Sci.* **2008**, *254*, 7143−7148.
(28) Caricato, A. P.; Cesaria, M.; Gigli, G.; Loiudice, A.; Luches, A.; Martino, M.; Resta, V.; Rizzo, A.; Taurino, A. Poly-(3-Hexylthiophene)/[6,6]-Phenyl-C_{61}-Butyric-Acid-Methyl-Ester Bilayer Deposition by Matrix-Assisted Pulsed Laser Evaporation for Organic Photovoltaic Applications. *Appl. Phys. Lett.* **2012**, *100*, 073306.
(29) Zhigilei, L. V.; Kodali, P. B. S.; Garrison, B. J. Molecular Dynamics Model for Laser Ablation of Organic Solids. *J. Phys. Chem. B* **1997**, *101*, 2028−2037.
(30) Colbourn, E. A., Ed. *Computer Simulation of Polymers*; Longman Scientific and Technical: Harlow, 1994.
(31) Morse, P. M. Diatomic Molecules According to the Wave Mechanics. II. Vibrational Levels. *Phys. Rev.* **1929**, *34*, 57−64.
(32) Morris, J. R.; Song, X. The Melting Lines of Model Systems Calculated from Coexistence Simulations. *J. Chem. Phys.* **2002**, *116*, 9352−9359.
(33) Ivanov, D. S.; Zhigilei, L. V. Combined Atomistic-Continuum Modeling of Short-Pulse Laser Melting and Disintegration of Metal Films. *Phys. Rev. B* **2003**, *68*, 064114.
(34) Garrison, B. J.; Itina, T. E.; Zhigilei, L. V. Limit of Overheating and the Threshold Behavior in Laser Ablation. *Phys. Rev. E* **2003**, *68*, 041501.
(35) Wu, C.; Zhigilei, L. V. Microscopic Mechanisms of Laser Spallation and Ablation of Metal Targets from Large-Scale Molecular Dynamics Simulations. *Appl. Phys. A: Mater. Sci. Process.* **2014**, *114*, 11−32.
(36) Bulgakova, N. M.; Bulgakov, A. V. Pulsed Laser Ablation of Solids: Transition from Normal Vaporization to Phase Explosion. *Appl. Phys. A: Mater. Sci. Process.* **2001**, *73*, 199−208.
(37) Gavish, B.; Gratton, E.; Hardy, C. J. Adiabatic Compressibility of Globular Proteins. *Proc. Natl. Acad. Sci. U.S.A.* **1983**, *80*, 750−754.
(38) Nagendra, H. G.; Sudarsanakumar, C.; Vijayan, M. Characterization of Lysozyme Crystals with Unusually Low Solvent Content. *Acta Crystallogr., Sect. D* **1995**, *51*, 390−392.
(39) Jacobs, W. M.; Nicholson, D. A.; Zemer, H.; Volkov, A. N.; Zhigilei, L. V. Acoustic Energy Dissipation and Thermalization in Carbon Nanotubes: Atomistic Modeling and Mesoscopic Description. *Phys. Rev. B* **2012**, *86*, 165414.
(40) Lide, D. R., Ed. *CRC Handbook of Chemistry and Physics*, 79th ed.; CRC Press: Boca Raton, FL, 1999.
(41) Because of a typo in the code, the actual value used in the simulations was $C^{exp} = 2.8 \times 10^{-3}$ eV/K.
(42) Gomez, J.; Hilser, V. J.; Xie, D.; Freire, E. The Heat Capacity of Proteins. *Proteins* **1995**, *22*, 404−412.
(43) Diller, R. Vibrational Relaxation During the Retinal Isomerization in Bacteriorhodopsin. *Chem. Phys. Lett.* **1998**, *295*, 47−55.
(44) Bu, L.; Straub, J. E. Simulating Vibrational Energy Flow in Proteins: Relaxation Rate and Mechanism for Heme Cooling in Cytochrome c. *J. Phys. Chem. B* **2003**, *107*, 12339−12345.
(45) Fujisaki, H.; Straub, J. E. Vibrational Energy Relaxation in Proteins. *Proc. Natl. Acad. Sci. U.S.A.* **2005**, *102*, 6726−6731.
(46) Smith, R. C.; Baker, K. S. Optical Properties of the Clearest Natural Waters (200−800 nm). *Appl. Opt.* **1981**, *20*, 177−184.
(47) Jollès, P. Lysozymes: A Chapter of Molecular Biology. *Angew. Chem., Int. Ed.* **1969**, *8*, 227−294.
(48) Kundrot, C. E.; Richards, F. M. Effect of Hydrostatic Pressure on the Solvent in Crystals of Hen Egg-White Lysozyme. *J. Mol. Biol.* **1988**, *200*, 401−410.
(49) Kocherbitov, V.; Arnebrant, T.; Söderman, O. Lysozyme-Water Interactions Studied by Sorption Calorimetry. *J. Phys. Chem. B* **2004**, *108*, 19036−19042.
(50) Urbassek, H. M.; Michl, J. A Gas-Flow Model for the Sputtering of Condensed Gases. *Nucl. Instrum. Methods Phys. Res., Sect. B* **1987**, *22*, 480−490.